10. Xia, J. L., Yadigaroglu, G., Liu, Y. S., Schmidli, J., and Smith, B. L., "Numerical and experimental study of swirling flow in a model combustor," Int. Journal of Heat and Mass Transfer, 41, No. 11, pp. 1485-1497, 1998.
11. Launder, B. E., "Second-moment closure: present and future," Int. J. Heat an Fluid Flow, 10, No. 4, pp. 282-300, 1989.
12. Magnussen, B. F., and Hjertager, B. H., "On mathematical modeling of turbulent combustion with special emphasis on soot formation and combustion," Computer Methods in Applied Mechanics and Engineering, 3, pp. 269-289, 1977.
13. Modest, M. F., Radiative Heat Transfer, Academic Press, 2003.
14. Lockwood, F. C., and Shah, N. C., "A new radiation solution method for incorporation in general combustion prediction procedures," Eighteenth Symposium (International) on Combustion Institute, pp.1405-1409, 1981.
15. Jeans, J. H., "The Equation of Radiative Transfer of Energy," Monthly Notices Royal Astronomical Society, 78, pp. 28-36, 1917.
16. Hottel, H. C., and Sarofim, A. F., Radiative Transfer, McGraw-Hill, New York, 1967.
17. Gupta, A. K., Lilley, D. G. and Syred, N., Swirl Flows, Abacus Press. Turnbridge Wells, 1984.
18. FLUENT User's Manual, Version 6.2.16, 2005.
19. Vandoormal, J. P. and Raithby, G. D., "Enhancements of the SIMPLE method for predicting incompressible fluid flows," Numerical Heat Transfer, 7, pp. 147-163, 1984.
20. Ohtsuka, M., "Numerical analysis of swirling non-reacting and reacting flows by the Reynolds stress differential method," International Journal of Heat and Mass Transfer, 388, No. 2, pp. 331-337, 1995.
21. German, A. E., and Mahmud, T., "Modeling of non-premixed swirl burner flows using a Reynolds-stress turbulence closure," Fuel, 84, pp. 583-594, 2005.
22. Warnatz, J., Maas, U., and Dibble, R. W., Combustion, Physical and Chemical Fundamentals, Modeling and Simulation, Experiments, Pollutant Formation, Fourth Edition, Springer, 2006.

چکیده فارسی

تاثیر مدل‌های انتقال گرمای تشعشعی بر پیش بینی شعله‌ی چرخشی متان- هوا در یک محفظه‌ی احتراق مدل توربین گاز

فرزاد بازدیدی تهرانی و حامد زینی وند
دانشگاه علم و صنعت ایران، دانشکده مهندسی مکانیک

در مقاله حاضر، به تحلیل عددی سه بعدی جریان واکنشی، چرخشی و دیفیوژنی متان و هوا در محفظه‌ی احتراق مدل یک توربین گاز مبتنی بر روش حجم محدود برای بررسی عملکرد دو مدل تشعشعی متداول، مدل انتقال مجزا (DTRM) و مدل تشعشعی P-1 پرداخته شده است. از مدل تنش‌های رینولدز (RSM) برای پیش‌بینی جریانات آشفته و از مدل اضمحلال گردابه (EDM) برای بررسی واکنش جریان بهره گرفته شده است. روش بالادست مرتبه دوم برای گسسته سازی جمله‌های جا به جایی تمام معادلات ترابری به کار رفته است. الگوی سیمپلسی برای کوپل کردت جمله‌های فشار و سرعت به کار رفته است. میانگین وزنی گازهای خاکستری (WSGGM) برای محاسبه‌ی خواص تشعشعی گازها استفاده شده است. نتایج عددی حاصل، در حالت اعمال انتقال گرمای تشعشعی و هم‌چنین بدون انتقال گرمای تشعشعی با نتایج تجربی معتبر موجود مورد مقایسه قرار گرفته و عملکرد دو مدل تشعشعی ذکر شده از دیدگاه قابلیت‌های محاسباتی و هم‌چنین دقت شبیه سازی ارزیابی شده است. مقایسه‌ی نتایج عددی، اهمیت نقش مدل‌های تشعشع را به ویژه در رابطه با محاسبه شار گرمایی وارد بر دیواره نشان می‌دهد. هر دو مدل تشعشعی انتقال مجزا و مدل P-1 در پیش‌بینی دمای گازهای درون محفظه، نتایج مشابهی را ارائه می‌دهند. اگر چه مدل انتقال مجزا زمان محاسباتی بسیار بیش‌تری نیاز دارد. مدل تشعشعی P-1 شار گرمایی وارد بر دیواره را بیش از میزان حقیقی پیش‌بینی می‌کند.

واژگان کلیدی: جریان واکنشی چرخشی، مدل اضمحلال ادی، مدل تنش‌های رینولدز، مدل تشعشعی

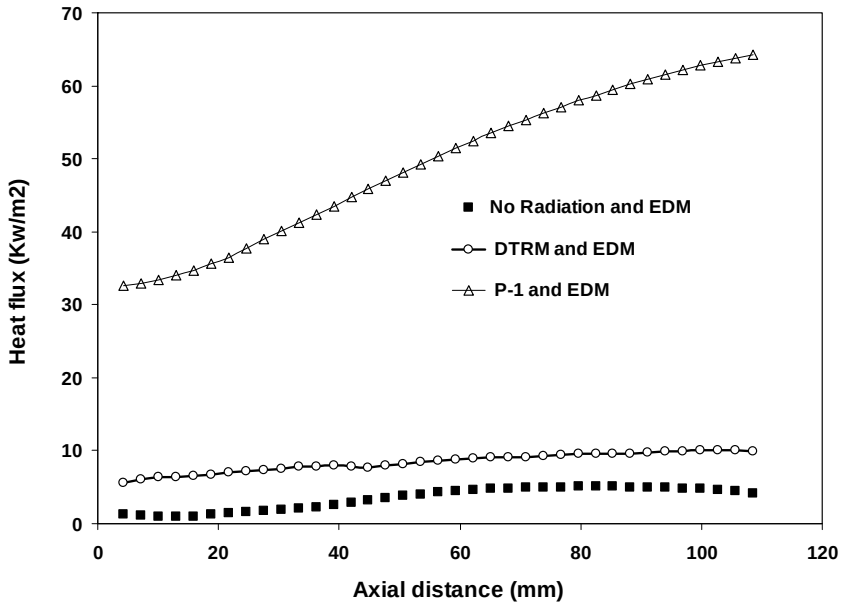

Figure 14. Total heat flux on walls along the axial distance of combustion chamber (with and without thermal radiation)

Concluding remarks

The main purpose of the present work is to numerically investigate the influence of two different thermal radiation models on the modeling of turbulent swirling non-premixed methane/air flame in a model gas turbine combustion chamber. Two models, namely, the DTRM and P-1 model are employed to predict the radiation heat transfer. The main conclusions are drawn as follows:

(1) The Reynolds stress turbulence model well predicts the combustor flow with a swirl number of 0.55. Two recirculation zones (central toroidal recirculation and corner recirculation zones) with two shear layers appear in the combustion chamber. The central toroidal recirculation zone attached to a reversed flow plays the main role in flame stability. Also, the corner recirculation zone increases the heat transfer to the walls.

(2) With the consideration of thermal radiation using both the present models, the predicted flame temperatures along the axial distance of the chamber are noticeably closer to the experimental data. Also, both radiation models predict temperature distribution across the chamber width reasonably well, displaying similar trends. Nevertheless, the use of DTRM involves a relatively high computational cost.

(3) The P-1 radiation model remarkably over-predicts the total heat flux on the walls. This is due to the presence of a local heat source in the combustion chamber.

References

1. Viskanta, R., and MengüÇ, M. P., Principle of Radiative Heat Transfer in Combustion Systems, Handbook of Heat and Mass Transfer, N. Cheremisinoff, Ed., Gulf Publishing, Houston, Vol. 4, Chap. 22, pp. 925-978, 1990.
2. Keramida, E. P., Liakos, H. H., Founti, M. A., Boudouvis, A. G., and Markatos, N. C., "Radiative heat transfer in natural gas-fired furnaces," International Journal of Heat and Mass Transfer, 43, pp. 1801-1809, 2000.
3. Jamaluddin, A. S., and Smith, P. J., "Predicting radiative transfer in axisymmetric cylindrical enclosure using the discrete ordinate method," Combustion Science and Technology, 62, pp. 173-186, 1995.
4. Ilbas, M., "The effect of thermal radiation and radiation models on hydrogen-hydrocarbon combustion modeling," International Journal of Hydrogen Energy, 30, pp. 1113-1126, 2005.
5. Sazhin, S. S., Sazhina, E. M., Faltsi-Saravelou, O., and Wild, P., "The P-1 Model for Thermal Radiation Transfer: Advantages and Limitations," Fuel, 75, pp. 289-294, 1996.
6. Stuttaford, P. A. and Rubini, P. A., "Assessment of a radiative heat transfer model for a new gas turbine combustor preliminary design tool," AIAA J. Propulsion and Power, 14, pp. 66-73, 1998.
7. Baek, S. W., Park, J. H., and Choi, C. E., "Investigation of droplet combustion with non-gray gas effects," Combustion Science and Technology, 142, pp. 55-79, 1999.
8. Weigand, P., Meier, W., Duan, X. R., Stricker, W., and Aigner, M., "Investigations of swirl flames in a gas turbine model combustor I: Flow field, structure, temperature, and species distributions," Combustion and Flame, 144, pp. 205-224, 2006.
9. Versteeg, H. K., and Malalasekera, W., An Introduction to Computational Fluid Dynamics: The Finite Volume Method, Addison Wesley-Longman, 1995.

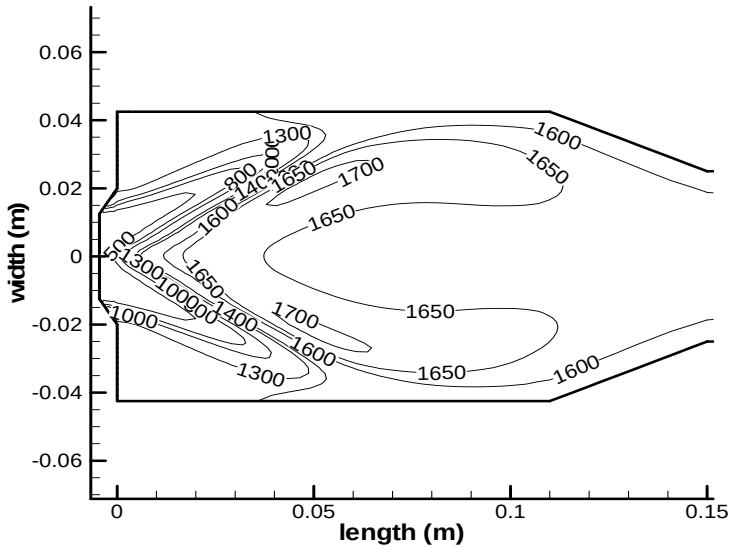

Figure 13-b. Temperature contours with DTRM thermal radiation model at axial section, $x = 0$

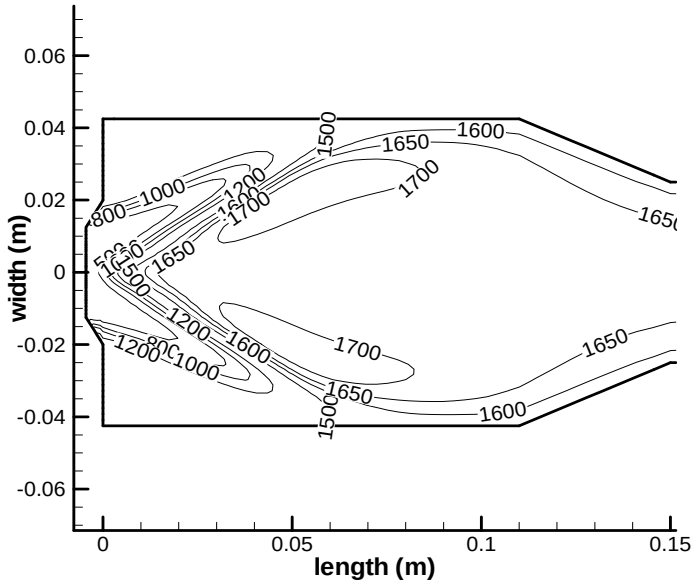

Figure 13-c. Temperature contours with P-1 thermal radiation model at axial section, $x = 0$

Fig. 14 demonstrates the profiles of total heat flux on the walls with and without consideration of the thermal radiation. The DTRM radiation model shows that the predicted total heat flux on the walls is enhanced (by a minimum factor of 2); hence the thermal radiation has a significant influence on the wall heat flux. Therefore, any disregard of the radiation mode of heat transfer causes a distinct error in the total heat flux calculations. On the other hand, the P-1 radiation model remarkably over-predicts the total heat flux on the walls. This is mainly due to the presence of a local heat source in the combustion chamber.

The DTRM can be recommended for simplified heat transfer analysis in combustion systems as it is a relatively simple model with respect to mathematical and implementational efforts. Its only disadvantage is its relatively high computational cost. The P-1 model is quite accurate for optically thick media, but it may yield inaccurate results for transparent media, especially near walls, and also when the radiation media are highly anisotropic; however, its convergence time is more favorable.

Fig. 12 shows the profiles of temperature along the axial distance of chamber. With the consideration of thermal radiation using both models, the predicted temperatures are noticeably closer to the experimental data. Negligible differences are observed between the predicted temperatures with and without radiation models near the furnace entrance. This is mainly because the combustion process is at an early stage, maintaining the mean temperature of this zone at low levels. However, as mentioned in Fig. 10, due to an overestimation of the temperature by the eddy dissipation model [22], the final predicted temperatures are shown to be higher than those of the experimental data especially near the walls. The difference between the present numerical data and the experimental data at the downstream is more distinct.

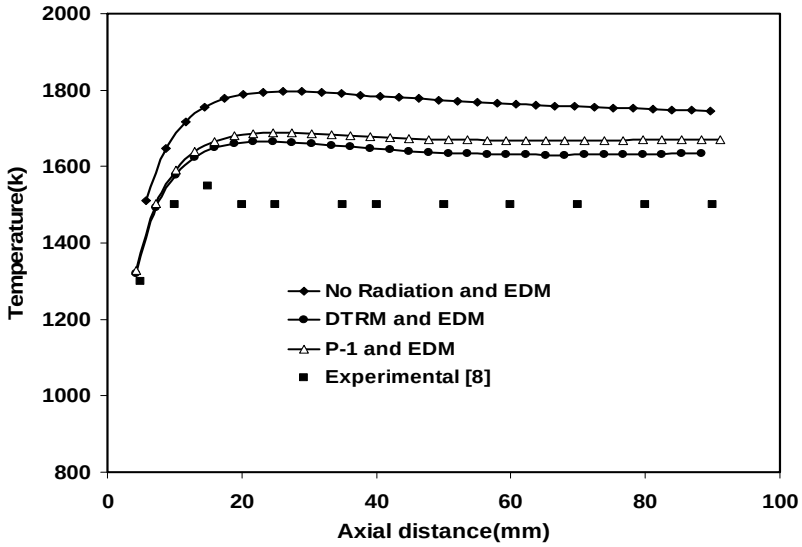

Figure 12. Temperature profiles along the axial distance

Temperature contours at the centre-line section of chamber ($x = 0$) without consideration of the thermal radiation and with two thermal radiation models are depicted in Figures 13a-c, respectively. As discussed before, it can clearly be seen that consideration of the effect of thermal radiation results in a decrease in the hot spot region in the combustion chamber. The maximum temperature is shown to decrease from approximately 1805K to 1650 K in this case. Adding radiation heat transfer to the other heat transfer mechanisms acting inside the combustion chamber renders the low temperature region produced by inlet air shorter. Fig 13a represents the temperature distribution of the longitudinal chamber cross section without radiation heat transfer.

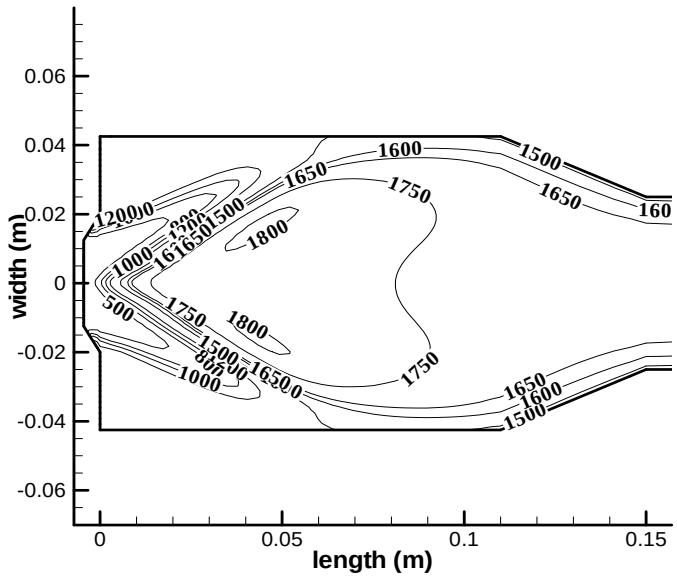

Figure 13-a. Temperature contours without thermal radiation at axial section, x = 0

Fig. 10 demonstrates the temperature profiles across the chamber width at height, $h = 5$ mm. The present reaction modeling (Eddy Dissipation Model, EDM), without consideration of thermal radiation, predicts relatively higher temperatures in the central region, where maximum temperature occurs. Nevertheless, due to the behavior of the flame such as blow off and partially premixed combustion, in a significant position (width between $r = 5$ mm and $r = 10$ mm) the present numerical results underestimate temperature. On the other hand, the EDM overestimates the temperature distribution in the maximum temperature region due to the ε / k term in its formulation. This term is over-predicted by the turbulence model (see Fig. 5) [20,21]. There is however a difference of approximately 6% between the experimental data and the present numerical results in the central (maximum temperature) region. The difference rises to nearly 15% on average at the width of $r = 5$ mm to $r = 10$ mm. In this region, the time scale of reaction is larger than that of mixing, which is contrary to the EDM assumptions cited in Section 4. In other words, the reaction is of finite rate whereas the EDM assumes an infinitely fast chemistry.

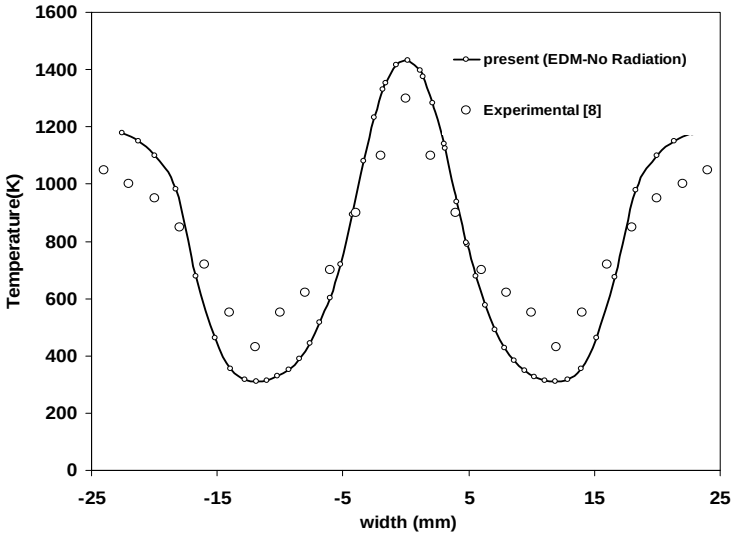

Figure 10. Temperature distribution across the chamber width at height, $h = 5$ mm

Fig. 11 illustrates the effect of consideration of thermal radiation on the present temperature distribution across the chamber width, at height, $h = 5$ mm. With the presence of thermal radiation, the agreement between the present results and available experimental data, especially in the central (maximum temperature) region, is reasonably well. Both the DTRM and P-1 radiation models display very similar trends for the temperature distribution. The radiation field in the present work is considered an isotropic medium which can make the P-1 model a reasonable model for the prediction of temperature distribution.

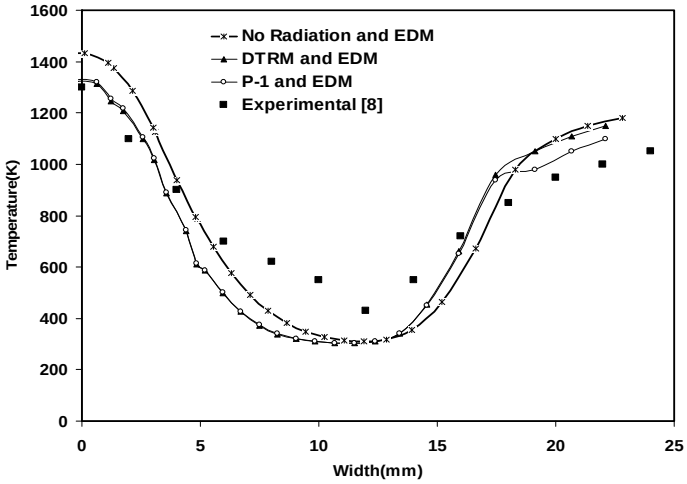

Figure 11. Temperature distribution across the chamber width, at height, $h = 5$ mm, with and without consideration of thermal radiation

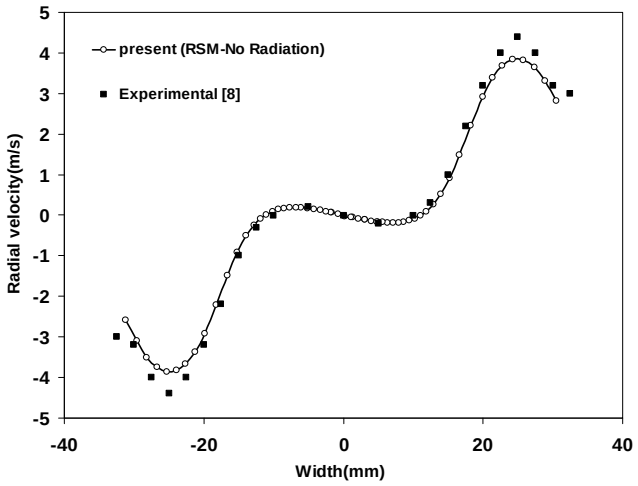

Figure 7. Profiles of radial velocity at height, $h = 30$ **mm**

Figures 8 and 9 represent the profiles of the tangential velocity across the chamber width at two different heights, $h = 1$ mm at $h = 30$ mm, respectively. It can be observed that the present predictions are within a reasonable difference of 10% on average, as compared with the experimental data. Although the RSM underestimates the tangential velocity, it predicts the flow trends (including the points of maximum and minimum) concerning the local tangential velocity sufficiently well.

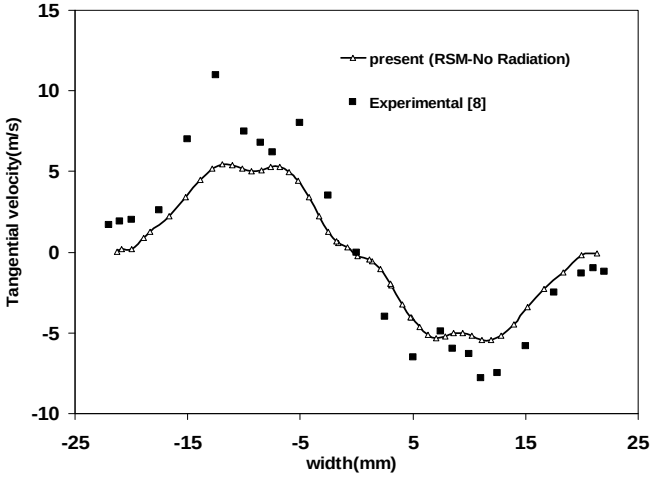

Figure 8. Profiles of tangential velocity at height, $h = 1$ **mm**

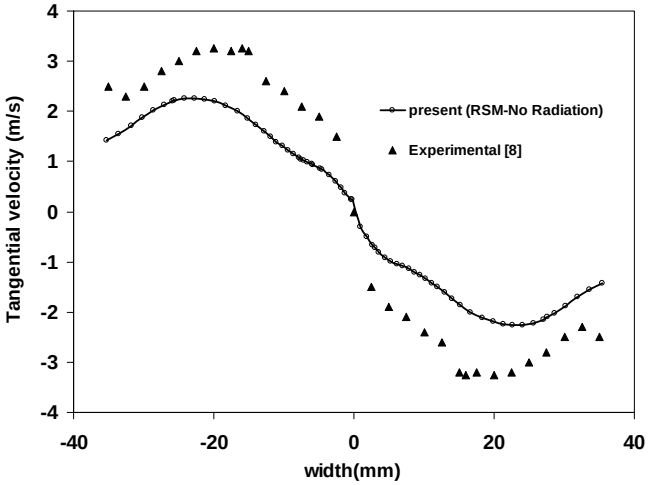

Figure 9. Profiles of tangential velocity at height, $h = 30$ **mm**

height, $h = 30$ mm is depicted. Fig. 7 displays the present radial velocity profiles across the chamber width at height, $h = 30$ mm. It can be seen that the RSM, in comparison to the experimental data, predicts the radial velocity of swirling flow quite well.

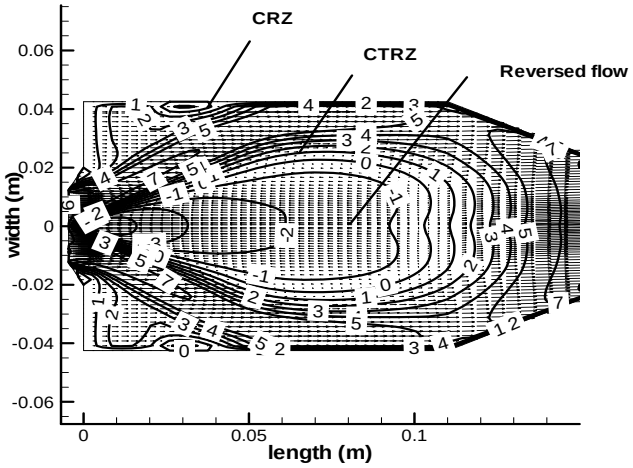

Figure 4. Axial velocity contours at center-line section, $x = 0$

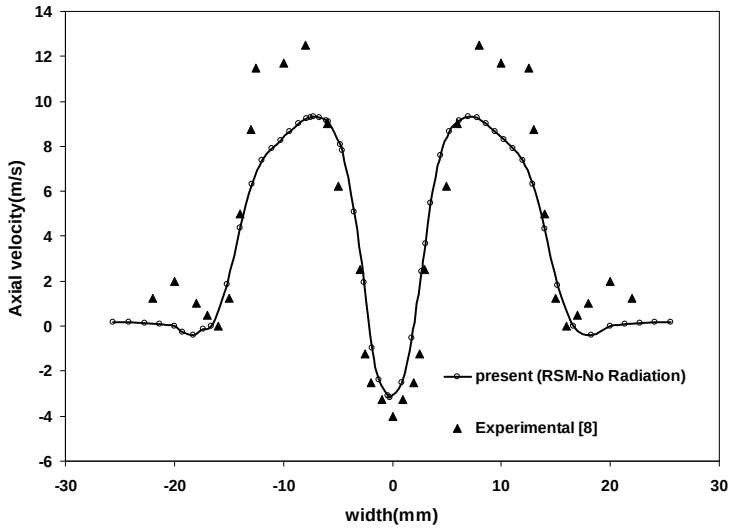

Figure 5. Profiles of axial velocity at height, $h = 1$ mm

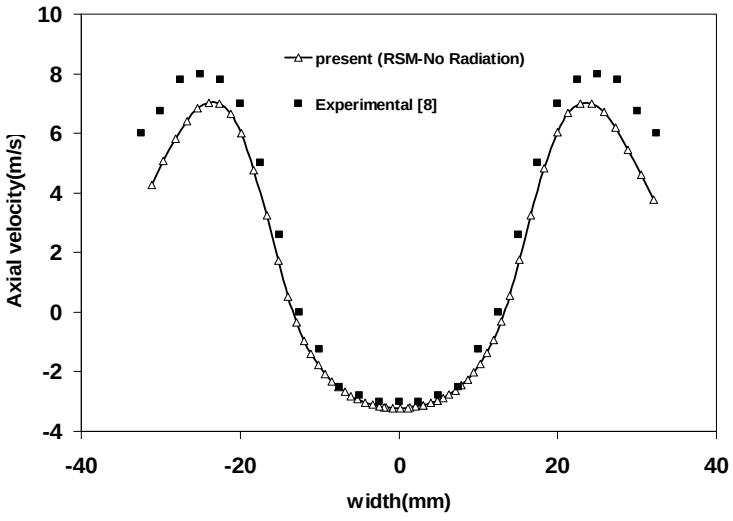

Figure 6. Profiles of axial velocity at height, $h = 30$ mm

Solution procedure

Due to the complexity of the present flow geometry, the finite volume based finite difference FLUENT code[18] is employed for solving the governing mean flow equations as well as the turbulence transport, fuel combustion and radiation model equations three-dimensionally. This code has been extensively validated against experimental data for many flow cases. A staggered grid arrangement is employed to solve the governing equations. The second-order upwind scheme is applied to the space derivatives of the advection terms in all transport equations. The flow field pressure-linked equations are solved by the SIMPLEC [19] algorithm. The convergence criterion is determined by the requirement that the maximum value of the normalized residuals of any equation must be less than 1×10^{-6} for energy and species terms, and about 1×10^{-5} for the other terms of the transport equations.

The grid spacing in the axial direction (z) is changed smoothly to minimize the deterioration of the formal accuracy of the discretization scheme, due to the variable grid spacing and in such a way that higher concentration of the nodes occurs near the inlet, reaction zone and the walls. The independence of the present solution from the grid size has been investigated thoroughly. As illustrated in Fig. 3, several different mesh sizes, within the range of 1×10^5 - 4×10^5, are examined. Finally, for enhanced accuracy, the finest 4×10^5 mesh size is selected throughout the present work.

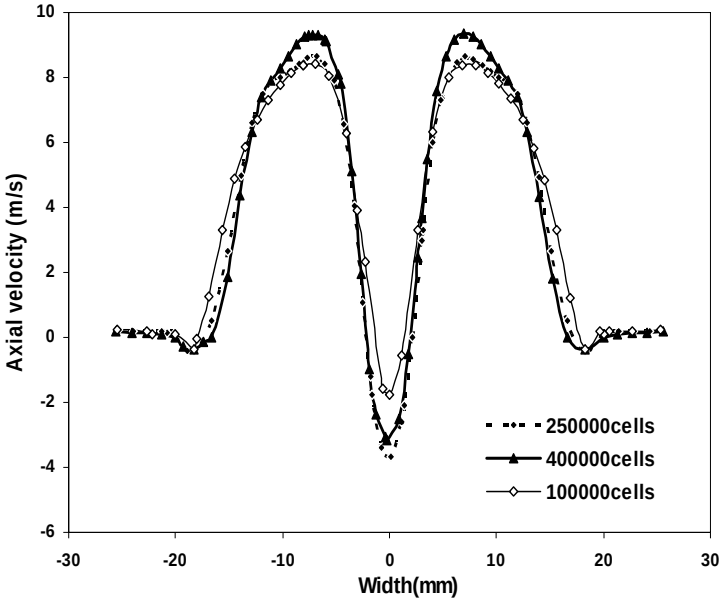

Figure 3. Independence of present solution from grid size: axial velocity at height, $h = 1$ mm, versus width

Results and discussion

Although the thermal radiation modeling is the main objective of the present research, correct prediction of the flow behavior is an important prerequisite for all the present results such as the temperature distribution and the effect of the radiation heat transfer.

Fig. 4 illustrates the axial (z-direction) velocity contours at the centre-line section of the combustion chamber, $x = 0$. Swirling flow with a pressure gradient causes two recirculation zones to appear at the centre and corner of the combustion chamber. The Central Toroidal Recirculation Zone (CTRZ) plays the main role for the flame stabilization and also the creation of the Corner Recirculation Zone (CRZ) increases the heat transfer to the walls. The CRZ appears just behind the expansion region of inlet stream. This along with the CTRZ attached to a reversed flow at the centre-line occur concurrently. Also, there are two shear layers between the central reversed flow and inlet stream and another between the CTRZ and inlet stream. The zero-axial velocity contours indicate the boundaries for the recirculation zones in the swirling flow field. Both the CTRZ and CRZ are shown in Fig. 4.

Fig. 5 shows a direct comparison of the present axial velocity profiles across the combustion chamber width with those of the available experimental results [8] at height, $h = 1$ mm. The turbulence RSM predicts the reversed flow reasonably well as compared with the experimental data. The maximum reversed flow occurs in the centre of combustor, $x = 0$. However, the maximum positive axial velocity is underestimated by the RSM, by approximately 20% on average, due to an over-prediction of the turbulence dissipation, ε [20-21]. Also, an underestimation of almost 5% for the maximum velocity is demonstrated in Fig. 6, where the axial velocity at

$$\varepsilon = C_{\mu}{}^{3/4}\,\frac{k^{3/2}}{l} \tag{30}$$

where,

$$l = 0.07\,L \tag{31}$$

U_{ref} , is inlet velocity and C_{μ} is equal to 0.09.

Other inlet boundary conditions can be represented as:

$$\begin{aligned} &\overline{u_1'^2} = k \\ &\overline{u_2'^2} = \overline{u_3'^2} = \frac{1}{2}k \\ &\overline{u_i' u_j'} = 0 \;(i \neq j) \end{aligned} \tag{32}$$

The necessary information about the present boundary conditions and fluid properties is presented in Table 1. Fig. 2 displays the model combustion chamber geometry including the computational grid. The computational domain comprising multi-blocks is meshed with hexahedral cells. The greatest concentration of the mesh is in the inlet and reaction zone.

Table 1- Input conditions and fluid properties

Geometry			
Fuel inlet zone (mm)	from $r = 7.5$	to $r = 7.87$	
Central air inlet zone (mm)	from $r = 0$	to $r = 7.5$	
Annular air inlet zone (mm)	from $r = 8.5$	to $r = 12.5$	
Combustor width (mm)	85		
Combustor length (mm)	114		
Inlet boundary conditions	Fuel	Central air	Annular air
Mass flow rate (kg/s)	0.00015	0.0019	0.0028
Turbulence kinetic energy (m^2/s^2)	2.05	1.242	1.242
Turbulence dissipation rate (m^2/s^3)	194.12	96.13	96.13
Temperature (K)	295	295	295
Swirl number	0	0.55	0.55
Pressure outlet (Pa)	101325		
Composition (mass fraction)			
O_2	0	0.2315	0.2315
N_2	0	0.7685	0.7685
CH_4	1	0	0

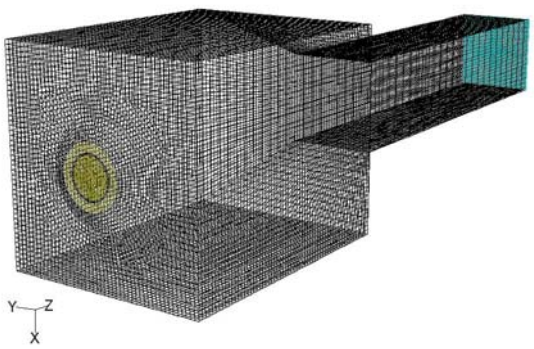

Figure 2. Geometry of model combustion chamber including the computational grid

Geometry and boundary conditions

The schematic view of the model combustion chamber is displayed in Fig. 1. The combustion chamber, according to the experimental setup of Weigand et al. [8], is cubic, and is modeled as a three-dimensional case. Co-swirling air at room temperature is supplied to the chamber through a central nozzle with a diameter of 15 mm and an annular nozzle with a inner diameter of 17 mm and an outer diameter of 25 mm, which contour to an outer diameter of 40 mm. The swirl number for air inlets is 0.55 and a non-swirling CH_4 gas is fed through 72 small channels, which in the present simulation are replaced with an annular nozzle with a slit width of 0.37 mm.

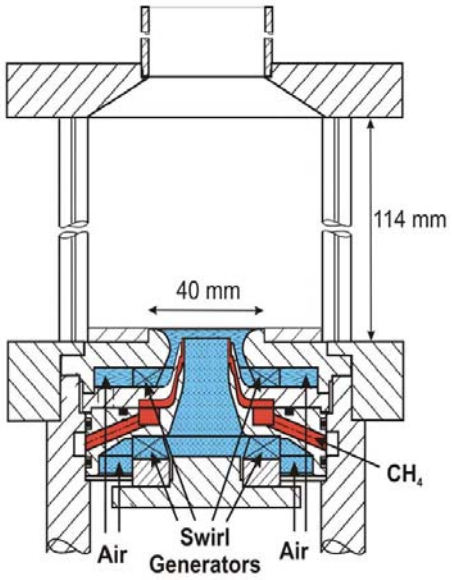

Figure 1. Schematic view of the model combustion chamber [8]

In recent modern gas turbine combustion chambers, swirling plays the main role in the production of mixing, enhancement of flame stability and decreasing emissions by providing a variable to control the flame intensity, shape and size. The swirl number is a non-dimensional parameter that characterizes the degree of swirl present in the flow. It is defined as in equation (26) [17]:

$$S = \frac{G_\theta}{L G_Z} \tag{26}$$

where, L is a characteristic length, typically chosen to be the exit radius of the burner. The terms G_θ and G_z are the axial flux of angular momentum and the axial flux of axial momentum, respectively. They are given in equations (27) and (28):

$$G_\theta = \int_0^\infty \rho u_z u_\theta r^2 dr \tag{27}$$

$$G_z = \int_0^\infty \rho u_z^2 dr \tag{28}$$

A swirl number of $S < 0.3$ known as a weak swirling flow and $S > 0.6$ as a strong swirling flow are common. For the present model, a swirl number of $S = 0.55$ is applied. For radiation calculations, the absorption coefficients used in the radiation models are taken as 0.6 and 0.2 for pure methane and air, respectively. The walls are treated as a gray heat sink of emissivity 0.8. The boundary conditions for P-1 approximations are derived from variational principles, and are strongly connected to the Marshak's boundary conditions [13]. The standard wall function is applied to the combustor walls. The boundary condition for the inlet is mass flow rate, and for the outlet is pressure outlet. First approximation for the k and ε can be obtained from the turbulence intensity, I, and a characteristic length, L, of the combustor (equivalent to combustor radius) by means of the following assumed forms [9]:

$$k = \frac{3}{2}(U_{ref} I)^2 \tag{29}$$

$$q_{in} = \int I_{in} s.n d\Omega \tag{17}$$

where, Ω is the hemispherical solid angle, I_{in} is the intensity of the incoming ray, s is the ray direction vector, and n is the normal pointing out of the domain. The net radiation heat flux from the surface, q_{out}, is then computed as a sum of the reflected portion of q_{in}, and the emissive power of the surface:

$$q_{out} = (1-\varepsilon_w) q_{in} + \varepsilon_w \sigma T_w^4 \tag{18}$$

where, T_w is the surface temperature of the point, P, on the surface.

Determining all traces of the rays and cells located along its way requires either a lot of computational time or a lot of memory. In addition, the vectorisation and parallelisation of the algorithms of ray-tracing radiation model is limited due to the different lengths of the individual rays.

P-1 radiation model

The P-1 model is the simplest case of a more general P-N model or spherical harmonic method, which is based on the expansion of the radiation intensity into an orthogonal series of spherical harmonics. This method is proposed by Jeans [15] who has studied the radiative transfer in the atmosphere. P-1 radiation model is one of the most attractive radiation models for industrial application. It has some advantages over the DTRM. It includes the effect of scattering; it is appropriate for complex geometries and its CPU time demand is much smaller. However, it also assumes that all surfaces are diffuse. The P-1 model tends to over-predict the radiative flux from localized heat sources or sinks. The radiation flux, q_r, for this model is obtained from the following equation:

$$q_r = -\frac{1}{3(a+\sigma_s) - C\sigma_s} \nabla G \tag{19}$$

where, a is absorption coefficient, σ_s is scattering coefficient, G is incident radiation and C is linear anisotropic phase function. For the calculation of local radiation intensity, the following relation is applied:

$$\nabla(\Gamma \nabla G) - aG + 4a\sigma T^4 = 0 \tag{20}$$

where, Γ is defined as in equation (21).

$$\Gamma = \frac{1}{(3(a+\sigma_s) - C\sigma_s)} \tag{21}$$

and the wall radiation heat flux is computed using the following equation in the P-1 model.

$$q_r.n = -\Gamma \nabla G.n \tag{22}$$

$$q_{r,w} = -\Gamma \frac{\partial G}{\partial n} \tag{23}$$

The flux of incident radiation at the wall is $q_{r,w}$. This model, as opposed to the DTRM, is unable to incorporate the global effects arising from properties at distant locations.

Weighted sum of gray gases model

The WSGGM approach is first introduced by Hottel and Sarofim [16]. In this model, the non-gray gas is replaced by gray gases for which the radiation heat transfer rates are calculated independently.

The total heat flux is then found by adding the heat fluxes of the gray gases after multiplication with certain weight factors. However, the total gas emissivity is approximated by the summation of a number of terms, each one being the multiplication of a weighting factor and a gray emissivity. The total emissivity and absorptivity are evaluated from the following equations:

$$\varepsilon = \sum_i^{Ng} a_{\varepsilon,i}(T) \left[1 - e^{-\kappa_i PS}\right] \tag{24}$$

$$a = \sum_i^{Ng} a_{\alpha,i}(T, T_\omega) \left[1 - e^{-\kappa_i PS}\right] \tag{25}$$

where, $a_{\varepsilon,i}$, $a_{a,i}$, κ_i and s are weighting factors, absorption coefficient of the ith gray gas and path length, respectively. The weighting factor may be a function of temperature. Modest [13] has shown that the WSGGM can be used with the turbulence-radiation interaction and therefore with any solution method of transfer equation (i.e., exact, P-N approximation, discrete transfer, discrete ordinate, etc.), provided that all boundaries are black and the medium is non-scattering.

while the reaction rate for (R2) becomes:

$$R_{CO} = \rho \frac{\varepsilon}{k} \min\left\{ aY_{CO}, a\frac{Y_{ox}}{s_2}, b\frac{Y_{CO_2}}{1+s_2} \right\} \tag{14}$$

where s_1 and s_2 are the stoichiometric mass ratio of oxygen to fuel and CO, respectively. The empirical constants a and b, amount to 4.0 and 0.5. This model assumes that the typical time scale of heat release, t_c, is much smaller than the turbulence time scale, $t_t = k/\varepsilon$ leading to $Da = t_t/t_c >> 1$. The Damkohler number, Da, describes the ratio of the macroscopic turbulence time scale to the flame characteristic time. When it is less than unity, it means that the chemistry is slow compared to the turbulent flow processes.

Radiation models

The Radiative Transfer Equation (RTE) for an absorbing, emitting and scattering medium at position r and in the direction s is given as [13]:

$$\frac{dI(r,s)}{ds} = -(a+\sigma_s)I(r,s) + an^2\frac{\sigma T^4}{\pi} + \frac{\sigma_s}{4\pi}\int_0^{4\pi} I(r,s')\Phi(s.s')d\Omega' \tag{15}$$

where r, s, s', s, a, n, σ_s, σ, I, T, Φ and Ω' are position vector, direction vector, scattering direction vector, path length, absorption coefficient, refractive index, scattering coefficient, Stefan-Boltzman constant (=5.672×10^{-8} W/m^{2}K^4), total radiation intensity (I depends on r and s), local temperature, phase function and solid angle, respectively. The RTE is an integro-differential equation for which exact solutions are not available for practical engineering applications. Multi-dimensionality, non-homogeneous media, and the spectral variation of radiative properties render solution of the RTE quite difficult.

However, reasonably accurate numerical solutions of the RTE may be obtained by introducing certain approximations. Since it is not possible to develop a single solution method that is applicable to a wide range of different systems, several solution methods with a varying degree of approximation have been developed according to the nature of physical system, characteristics of the medium, the degree of accuracy required and the availability of computer hardware facilities. The major methods can be summarized as follows [1]: (1) statistical methods, (2) the zonal method, (3) flux methods, including the discrete ordinate approximation (4) moment methods, (5) spherical harmonic approximation, and (6) hybrid methods. In the present work, the performance of DTRM, as a statistical method and P-1 radiation model, as a spherical harmonic approximation has been assessed. A brief description of each model is presented in the following sections. For further details, the reader is referred to [1, 13].

Discrete transfer radiation model

The DTRM is developed by Lockwood and Shah [14]. It discretizes the RTE along rays similar to the Monte Carlo method [13]. Among its advantages, the accuracy can be increased by simply increasing the number of rays. Its disadvantages are that the model assumes all surfaces are diffuse, radiation is gray and the effect of scattering is excluded. Also, for a large number of rays the CPU time demand becomes intensive. The DTRM involves the calculation of the radiation heat transfer along a number of predetermined paths using a recurrence equation. The radiation intensity entering and leaving each cell along a path is calculated for each ray, enabling the cell source term to be determined. Calculations are performed from wall to wall and an estimated initial intensity is used to initiate the calculation at the walls. The boundary conditions are then used to update the wall intensities and the procedure is iterative. Within the cells the properties are assumed to be uniform. The calculation procedure is based on ray tracing and takes into account all the local temperature and gas property values along a ray path. The method, therefore, incorporates not only the local properties but also the global effects arising from properties at distant locations. Also, the model accuracy strongly depends on the number of rays for every cell. In the present work, 16 rays have been considered for each cell.

The equation for the change of radiant intensity, dI, along a path, ds, may be written as:

$$\frac{dI}{ds} + aI = \frac{a\sigma T^4}{\pi} \tag{16}$$

where, a, I, T and σ are gas absorption coefficient, intensity, local gas temperature and Stefan-Boltzmann constant, respectively. The WSGGM, as outlined in the following section, is applied to calculate the absorption coefficient according to the pressure, temperature and species variant

The radiation intensity approaching a point on a wall surface is integrated to yield the incident radiation heat flux, q_{in}, as in equation (17).

equation and the concept of an isotropic eddy viscosity is no longer needed. The abbreviated form of the RSM is written as follows [9]:

$$\frac{\partial(\rho U_k \overline{u_i u_j})}{\partial x_k} = \left(P_{ij} - \varepsilon_{ij} + \phi_{ij} + d_{ijk}\right) \tag{5}$$

where, P_{ij}, ε_{ij}, ϕ_{ij} and d_{ij} are production, dissipation, pressure-strain and diffusion of Reynolds stresses, respectively. The Reynolds stress diffusion includes two terms: Turbulent diffusion, d_{ij}^{T} and molecular diffusion d_{ij}^{L}. The fundamental terms in the Reynolds stress transport equations are mentioned in the following equations:

$$d_{ij}^{T} = -\frac{\partial}{\partial x_k} = \left[\rho\overline{u_i u_j u_k} + \overline{p\left(\delta_{kj}u_i + \delta_{ik}u_j\right)}\right] \tag{6}$$

$$d_{ij}^{L} = -\frac{\partial}{\partial x_k}\left[\mu\frac{\partial}{\partial x_k}\left(\overline{u_i u_j}\right)\right] \tag{7}$$

$$P_{ij} = -\rho\left(\overline{u_i u_k}\frac{\partial U_j}{\partial x_k} + \overline{u_j u_k}\frac{\partial U_i}{\partial x_k}\right) \tag{8}$$

$$\phi_{ij} = \overline{p\left(\frac{\partial u_i}{\partial x_j} + \frac{\partial u_j}{\partial x_i}\right)} \tag{9}$$

$$\varepsilon_{ij} = -2\mu\overline{\frac{\partial u_i}{\partial x_k}\frac{\partial u_j}{\partial x_k}} \tag{10}$$

However, d_{ij}^{T}, ε_{ij} and ϕ_{ij} need to be modeled so as to close the equations. The d_{ij}^{T} term can be modeled by the gradient-diffusion model with a scalar turbulent diffusivity.

$$d_{ij}^{T} = \frac{\partial}{\partial x_k}\left(\rho\frac{\nu_t}{\sigma_k}\frac{\partial\overline{u_i u_j}}{\partial x_k}\right) \tag{11}$$

where ν_t can be computed from equation (12), and where σ_k is equal to 0.82.

$$\nu_t = C_\mu\frac{k^2}{\varepsilon} \tag{12}$$

where C_μ is dimensional constant equal to 0.09, and k and ε are turbulence kinetic energy and dissipation, respectively.

Combustion model

In the present study, combustion is modeled as a two-step mechanism, where production and combustion of carbon monoxide is taken into account. In the first stage, fuel is oxidized into carbon monoxide and water vapor, while in the second stage carbon monoxide oxidizes into carbon dioxide:

$$CH_4 + \frac{3}{2}O_2 \rightarrow CO + 2H_2O \tag{R1}$$

$$CO + \frac{1}{2}O_2 \rightarrow CO_2 \tag{R2}$$

The Eddy Dissipation Model (EDM) proposed by Spalding and then modified by Magnussen and Hjertager [12] is applied. Therefore, two additional transport equations for fuel and oxidizer need to be solved. In addition, the temperature, deduced from the enthalpy field, is obtained from a transport equation. The reaction rates of CH_4 and CO can be considered to be proportional to the turbulence time scale (ε/k) as well as to the smallest mass fraction of the fuel, oxygen and products concentration for equation (13), and carbon monoxide, carbon dioxide and oxygen concentration for equation (14).The reaction rate for (R1) is then represented by:

$$R_{fu} = \rho\frac{\varepsilon}{k}\min\left\{aY_{fu}, a\frac{Y_{ox}}{s_1}, b\frac{Y_P}{1+s_1}\right\} \tag{13}$$

applied to an optically thin enclosure with localized sources of heat. Stuttaford and Rubini [6] have evaluated the performance of DTRM for the prediction of thermal radiation and preliminary design of a new gas turbine combustor. Computational fluid dynamics is of great interest to researchers and designers due to the complexity of combustion and heat transfer phenomena. Non-premixed flames have widely been used in industrial process systems such as burners, gas turbine combustors, boilers utility and furnaces. Many researchers have investigated a turbulent diffusion flame numerically and/or experimentally. Suitable model simulation can be applied in the design of burners and gas turbines. On the other hand, considerable efforts have recently been made for developing useful and accurate methods of modeling the non-gray behavior of typical product gases such as CO_2 and H_2O. Among others, the Weighted Sum of Gray Gases Model (WSGGM), which replaces the non-gray gas by an equivalent finite number of gray gases, is known to be a simplified but reasonably practical as well as accurate model for engineering applications. Baek et al. [7] have used the FLUENT code to investigate the capability of the extended WSGGM in a liquid fuel combustion chamber. They have compared their results with gray gas and non-gray gas assumptions.

The main purpose of the present work is to investigate the influence of two different thermal radiation models on the modeling of turbulent swirling diffusion methane/air flame in a model gas turbine combustor. The two radiation models, namely, the DTRM and P-1 model are employed to predict the radiation heat transfer. Present predictions are compared with the experimental data of Weigand et al. [8] who have used Laser Doppler Velocimetry (LDV) and Planar Laser-Induced Fluorescence (PLIF) techniques for flow measurements and flame structure visualization.

Governing equations

Turbulent reacting flows under steady-state and incompressible conditions are governed by Favre-averaging equations, represented as follows [9]:

Mass

$$\frac{\partial\left(\rho\overline{U_j}\right)}{\partial x_j}=0 \tag{1}$$

Momentum

$$\frac{\partial\left(\rho\overline{U_i}\overline{U_j}\right)}{\partial x_j}=-\frac{\partial P}{\partial x_i}+\frac{\partial}{\partial x_j}\left[\mu\frac{\partial\overline{U_i}}{\partial x_j}-\rho\overline{u_i''u_j''}\right] \tag{2}$$

Energy

$$\frac{\partial}{\partial x_i}\left(\rho u_i\bar{h}\right)=\frac{\partial}{\partial x_i}\left(k_{eff}\frac{\partial\bar{T}}{\partial x_i}-\sum_j h_j J_j+u_j\left(\tau_{ij}\right)_{eff}\right)+S_h \tag{3}$$

Species

$$\frac{\partial}{\partial x_i}\left(\rho u_i\overline{Y_n}\right)=-\frac{\partial J_{i,n}}{\partial x_i}+R_n \tag{4}$$

where, ρ in equations (3) and (4) represents density, and is obtained from the ideal gas law equation. x_j is the coordinate, μ is the dynamic viscosity and U_j and u_j are the mean and the corresponding fluctuation velocity component in the j direction, respectively. In equation (3), k_{eff} is the effective conductivity ($k_{eff}=k+k_t$, where k is the sum of conductivity and k_t is the turbulent conductivity of the fluid). J_j is the diffusion of species, n, and $\left(\tau_{ij}\right)_{eff}$ is the effective stress tensor defined in the same way as the effective conductivity. The first three terms on the right hand side of equation (3), represent energy transfer in turn due to conduction, species diffusion and viscous dissipation. S_h includes the heat of chemical reaction or any other heat sources present. In equation (4), Y_n is the mass fraction of species n, and R_n is the production rate of species n, which, for a laminar flow, can be obtained using the Fick's law.

Turbulence model

Due to the anisotropic behavior of a swirling flow, isotropic models are unable to predict this type of flow correctly [10]. Hence, in the present work, the Reynolds Stress Model (RSM) is applied as an anisotropic model proposed by launder et al. [11]. In the RSM, the Reynolds stresses are calculated from their own transport

Journal of Fuel and Combustion
Vol. 1, No. 2, Fall 2008 - Winter 2009

Influence of Thermal Radiation Models on Prediction of Reactive Swirling Methane/Air Flame in a Model Gas Turbine Combustor

F. Bazdidi-Tehrani[*] and H. Zeinivand[**]
Department of Mechanical Engineering, Iran University of Science and Technology
(Receipt: 23/08/2008, Accepted: 26/04/2009)

A numerical simulation of reactive swirling methane/air non-premixed flame in a new three-dimensional model combustion chamber is carried out to assess the performance of two thermal radiation models, namely, the Discrete Transfer Radiation Model and the P-1 Model. A Finite Volume staggered grid approach is employed to solve the governing equations. The second-order upwind scheme is applied for the space derivatives of the advection terms in all transport equations. The SIMPLEC algorithm is used to handle the velocity and pressure coupling. The eddy dissipation model is employed to predict the heat release and the Reynolds stress turbulence model is applied to simulate the flow behavior. A weighted-sum-of-gray-gases model is used for the gas radiative properties. Computational results with and without the radiation effects are compared with the available experimental data and the two radiation models are evaluated in terms of computational efficiency and prediction accuracy. Comparison of present numerical results with experimental data reveals that the thermal radiation mode is important especially for heat flux on the walls. Both the Discrete Transfer Radiation and P-1 radiation models predict temperature distribution reasonably well, although the latter involves a relatively high computational cost. The P-1 model overestimates heat flux on the walls.

Key Words: Reactive swirling flow, Eddy dissipation model, Reynolds stress model, Radiation model

Introduction

For many combustion processes, thermal radiation is the dominant energy transport mechanism to surrounding surfaces. Thermal radiation can have a significant effect on the important issue of NO formation, due to the sensitivity of the thermal NO kinetics to temperature. On the other hand, most mathematical models for capturing NO concentration are based on the temperature distribution. However, the modeling of radiation heat transfer is often neglected in a combustion analysis, mainly because it involves complex mathematics and high computational costs. The accuracy of the radiation calculation depends on a combination of both the calculation technique and the level of accuracy to which the properties of the radiating media and surrounding walls are determined. A large bulk of literature relevant to this subject exists.

Viskanta and Mengüc [1] have made a well-known review on the radiative heat transfer properties and models in the combustion systems and emphasized that thermal radiation plays an important role not only in large and intermediate, but also in small combustion systems. They also have compared several thermal radiation models and shown that lower-order spherical harmonics approximations generally yield more accurate results if the radiation field in the medium is almost isotropic. Keramidia et al. [2] have numerically evaluated two radiation models, namely, the discrete transfer radiation model, and the six flux model for a two dimensional natural gas-fired furnace. Their results have confirmed that the effect of thermal radiation on flame temperature predictions is significant. Both models have shown good agreement with the experimental data. The Discrete Transfer Radiation Model (DTRM) has been reported to predict results more accurately with less sensitivity to optical properties, but it requires its own geometrical description, and also is computationally more expensive. Jamaluddin and Smith [3] have numerically used the discrete ordinate method to predict the radiation heat transfer in an axisymmetric cylindrical enclosure. Ilbas [4] has investigated the capability of discrete transfer radiation and P-1 models for thermal radiation modeling in hydrogen-hydrocarbon combustion. He has demonstrated that ignoring the thermal radiation causes significant errors in the overall prediction, especially in the NO formation. In the hydrocarbon fuel combustion, the products H_2O, CO and CO_2 are particularly important owing to their comparatively high absorptivities and emissivities in the near infrared region. In a system containing combustion gases, the emission from the molecules of H_2O and CO_2 dominate, and the effects of the remaining constituents are small enough to be considered negligible.

Sazhin et al. [5] have applied the P-1 radiation model for a combustion problem to investigate its advantages and limitations by employing the FLUENT code. They have mentioned that the P-1 model is applicable both for optically thick and optically thin media. Nevertheless, caution is needed when the model is

[*] Associate Professor- Corresponding author (Email: bazdid@iust.ac.ir)
[**] M. Sc. in Energy Conversion (Email: hamedzeinivand@yahoo.com)